Neurosci. Bull. August, 2022, 38(8):871–886
https://doi.org/10.1007/s12264-022-00848-3

www.neurosci.cn
www.springer.com/12264

ORIGINAL ARTICLE

Intestinal Dopamine Receptor D2 is Required for Neuroprotection Against 1-Methyl-4-phenyl-1,2,3,6-tetrahydropyridine-induced Dopaminergic Neurodegeneration

Hairong Peng[1,2] · Shui Yu[1,2] · Yukai Zhang[1,2] · Yanqing Yin[1] · Jiawei Zhou[1,2,3]

Received: 26 September 2021 / Accepted: 26 December 2021 / Published online: 11 April 2022

Abstract A wealth of evidence has suggested that gastrointestinal dysfunction is associated with the onset and progression of Parkinson's disease (PD). However, the mechanisms underlying these links remain to be defined. Here, we investigated the impact of deregulation of intestinal dopamine D2 receptor (DRD2) signaling in response to 1-methyl-4-phenyl-1,2,3,6-tetrahydropyridine (MPTP)-induced dopaminergic neurodegeneration. Dopamine/dopamine signaling in the mouse colon decreased with ageing. Selective ablation of *Drd2*, but not *Drd4*, in the intestinal epithelium, caused a more severe loss of dopaminergic neurons in the substantia nigra following MPTP challenge, and this was accompanied by a reduced abundance of succinate-producing *Alleoprevotella* in the gut microbiota. Administration of succinate markedly attenuated dopaminergic neuronal loss in MPTP-treated mice by elevating the mitochondrial membrane potential. This study suggests that intestinal epithelial DRD2 activity and succinate from the gut microbiome contribute to the maintenance of nigral DA neuron survival. These findings provide a potential strategy targeting neuroinflammation-related neurological disorders such as PD.

✉ Jiawei Zhou
jwzhou@ion.ac.cn

[1] Institute of Neuroscience, State Key Laboratory of Neuroscience, CAS Center for Excellence in Brain Science and Intelligence Technology, Chinese Academy of Sciences, Shanghai 200031, China

[2] School of Future Technology, University of Chinese Academy of Sciences, Beijing 100049, China

[3] Shanghai Center for Brain Science and Brain-Inspired Intelligence Technology, Shanghai 201210, China

Keywords Intestine · DRD2 · Parkinson's disease · MPTP · Succinate · Mitochondria

Introduction

Prolongation of the lifespan is a success of modern science and technology. However, aging is a primary risk factor for most neurodegenerative diseases, such as Alzheimer's disease (AD) and Parkinson's disease (PD) [1–3]. PD is the second most common neurodegenerative condition after AD, affecting 2%–3% of the population >65 years old. PD is caused by progressive dopaminergic (DAergic) neuron loss in the substantia nigra (SN) [4–6]. In addition to motor deficits, many patients with PD develop non-motor symptoms, such as constipation, depression, and rapid-eye-movement sleep behavior disorder [7]. These symptoms generally occur years before the onset of motor symptoms [8]. In the last several years, these prodromal symptoms have attracted much attention in terms of their relation to and potential impact on the early diagnosis and treatment of PD.

Numerous studies have indicated that the pathogenesis of PD mainly involves several processes, such as impaired mitochondrial respiration, oxidative stress, disruption of Ca^{2+} homeostasis, misfolded α-synuclein aggregation, and glia-mediated neuroinflammation [9], some of which are known as hallmarks of the aged brain [1, 10–12]. Recent studies have demonstrated that misfolded α-synuclein aggregates that form Lewy bodies and Lewy neurites are detected in the enteric nervous system before clinical diagnosis [7, 13], suggesting that the disruption of gastrointestinal homeostasis may play an important role in the progression of PD [8, 14]. It remains to be understood

whether and how gastrointestinal pathology contributes to PD pathogenesis.

The gut microbiota is physically independent but functionally associated with the gut *per se*. During ageing, the gut microbiota remarkably influences the structure and function of the gastrointestinal system, reciprocally. Previous studies have revealed that the individual gut microbiota of fecal samples exhibits distinct profiles, and this inter-individual variation is greater in older adults, as evaluated using 16S ribosomal DNA sequencing [15]. A shift in the microbiota toward a Bacteroidetes-predominated population in frailer older individuals compared to younger individuals has also been reported [3]. Moreover, there is evidence that PD patients display gut microbiota dysbiosis which can trigger the inflammation-induced misfolding of α-synuclein in the intestine [13, 16, 17] and several kinds of pathogenic α-synuclein propagate to the brain *via* the vagus nerve to cause PD in rodents. However, whether the gut or microbiota plays an alternative role in the maintenance of nigral DA neuron survival remains elusive [16, 18–22].

Dopamine (DA) is one of the major neurotransmitters that play a crucial role in a variety of physiological activities, such as movement control, learning and memory, and reward-motivated behavior [23]. Deregulation of DA signaling is involved in various pathological processes, such as PD and addiction. DA exerts its function *via* its five G-protein coupled receptors that are divided into two types: D1-like and D2-like receptors. D1-like receptors, DRD1 and DRD5, share 80% amino-acid sequence, while D2-like receptors are less homologous [23]. Although the role of DA in brain activities has been well documented in the past few decades, knowledge of intestinal DAergic signaling is rather limited. It appears that bacteria are one of the major sources of DA in the gut, as there is evidence that germ-free mice exhibit a substantial reduction in levels of free active DA in the cecal and colonic lumen [24]. The DA in the gut may be derived from up to one dozen bacteria, such as *Klebsiella pneumoniae*, *Bacillus cereus*, *B. mycoides*, *B. subtilis*, *Escherichia coli*, *Hafnia alvei*, *Proteus vulgaris*, *Serratia marcescens*, *Staphylococcus aureus,* and *Morganella morganii*, according to an *in vitro* study [25]. Notably, in addition to DA, *M. morganii* also produces multiple biogenic amines, including tyramine and phenethylamine, which can activate D2-like receptors, but not D1-like receptors [26], implying the complex nature of the regulation of DA receptor signaling in the gut [26].

Moreover, these DA-producing bacteria have been implicated in PD pathogenesis. It has been shown that the relative abundance of the genus *Klebsiella* and *Staphylococci* is decreased in older people [27] and the genus *Klebsiella* is also decreased in subjects with PD [28]. Interestingly, administration of *B. subtilis* inhibits α-synuclein aggregation and clears preformed aggregates in a *C. elegans* model of synucleinopathy [28], indicating that the DA-associated gut microbiota plays an important role in modulating the degenerative process in PD. However, the exact role of gut DA signaling in PD pathogenesis remains largely unknown.

In the present study, we aimed to investigate the contribution of intestinal DRD2 signaling to MPTP-induced neurodegeneration. We identified an intestinal epithelial DRD2-dependent mechanism for succinate control of nigral DA neuron survival as a crucial signaling axis in the maintenance of nigral DA integrity. We showed that selective deficiency of *Drd2* in the intestinal epithelium caused significant perturbation of gut microbiota, including succinate-producing *Alleoprevotella*, resulting in a marked decrease in the survival of nigral DAergic neurons following exposure to the neurotoxin MPTP. These data suggest that intestinal DRD2 is crucial for maintaining the integrity of the SN in PD

Materials and Methods

Animals

Adult (2–6 months old) C57BL/6 mice were purchased from the Shanghai Laboratory Animal Center, Chinese Academy of Sciences. *Drd2*-floxed mice were created by the Shanghai Research Center for Model Organisms (Shanghai, China) [29]. Briefly, the floxed *Drd2* allele was generated by introducing loxP sites flanking exon 2 of the *Drd2* locus into the mouse genome. *Drd4*-floxed mice were created by the Beijing Biocytogen Co., Ltd (Beijing, China). Briefly, the floxed *Drd4* allele was generated by introducing loxP sites flanking exon 1 of the *Drd4* locus into the mouse genome. Characterization and genotyping of mice heterozygous for the floxed *Drd2* allele ($Drd2^{flox/+}$) were described previously [29]. Genotyping was performed using the following primers: *Drd4*-loxP forward, 5'-ATTGCCATGTGTCCAGCAAG-3', reverse, 5'-CCTGCCTCTTGACTTAGGTCTTC-3'. Vil1-cre transgenic mice were purchased from the Jackson Laboratory (Stock No. 021504). They were maintained on a 12-h light/dark cycle at 23°C with food and water available *ad libitum*. Five mice were housed in a cage. All mice were on the C57BL/6 background and were kept in a specific pathogen-free facility at the Institute of Neuroscience. All procedures were approved by the Animal Care and Use Committee of the Institute of Neuroscience, Chinese Academy of Sciences.

MPTP Challenge and Succinate Treatment

MPTP was injected as described previously [30, 31]. In brief, male *Drd2*^{vil1} cKO mice or *Drd4*^{vil1} cKO mice (2–6 months old) and their littermates (WT) were administered MPTP (20 mg/kg, dissolved in saline, i.p.) every 2 h, four times. Seven days after injection, mice were sacrificed and brain tissue was taken for various analyses.

In order to test whether succinate exerts a neuroprotective effect on DA neurons in MPTP-treated mice, adult male C57BL/6 mice (2–6 months old) were administered succinic acid disodium salt (Sigma-Aldrich, 224731, i.p.) *via* both intraperitoneal injection (590 mg/kg, once daily) and in drinking water (1 mg/mL) for 5 consecutive days. Three days after treatment with succinate, the animals received MPTP injection as described above and were sacrificed after 7 days.

Immunohistochemical Staining and Cell Counting

Seven days after MPTP injection, mice were anesthetized and perfused with 4% paraformaldehyde. Cryosections were incubated with rabbit anti-TH pAb (1:800; Chemicon) followed by incubation with biotinylated secondary antibody. The same sections were then incubated with A/B solution (Vectastain ABC kit, Peroxidase, PK-4000). After that, brain slices were transferred to a 3,3′-diaminobenzidine solution and incubated for 2 min with 3% H_2O_2. To analyze the TH^+ cell number in the SN, we counted TH^+ cells in 10 brain slices as described previously [30, 31].

16S RNA Sequencing

Mouse fecal pellets were collected before MPTP injection and 7 days after MPTP injection and stored at –80°C until use. Microbial community genomic DNA was extracted from the fecal samples using the E.Z.N.A.® soil DNA Kit (Omega Bio-Tek, Norcross, GA, USA) according to the manufacturer's instructions. Briefly, the DNA quality was checked on 1% agarose gel, and DNA concentration and purity were determined with a NanoDrop 2000 UV-vis spectrophotometer (Thermo Scientific, Wilmington, USA). The hypervariable region V3-V4 of the bacterial 16S rRNA gene was amplified with primer pairs 338F (5'-ACTCCTACGGGAGGCAGCAG-3') and 806R (5'-GGACTACHVGGGTWTCTAAT-3') by an ABI GeneAmp® 9700 PCR thermocycler (ABI, CA, USA). Purified equimolar amplicons were pooled and paired-end sequenced on an Illumina MiSeq PE300 platform/NovaSeq PE250 platform (Illumina, San Diego, USA) according to the standard protocols by Majorbio Bio-Pharm Technology Co. Ltd. (Shanghai, China). The data were analyzed on the free online platform Majorbio Cloud Platform (www.majorbio.com) of Shanghai Majorbio Bio-pharm Technology Co., Ltd.

Isolation of Intestinal Epithelial Cells

Intestinal epithelial cells (IECs) were isolated as described previously by Pan *et al.* [32]. Briefly, mice were anesthetized and sacrificed. The intestine was cut longitudinally to remove gross debris. The tissue was fragmented into small pieces that were washed in ice-cold PBS and then transferred to sterile PBS freshly supplemented with 0.01 mol/L EDTA. The epithelial layer was separated from the underlying lamina propria for 15 min at 37°C in a rotisserie rack with end-over-end rotation. IECs were then harvested after centrifugation.

Bulk RNA Sequencing

Isolation of total RNA, RNA-sequencing analysis, and bioinformatics analysis were performed as described previously [33]. Briefly, the substantia nigra tissue of *Drd2*^{vil1} cKO and their littermates or isolated IECs were homogenized in TRIzol reagent (Invitrogen, Carlsbad, California, USA). Total RNA was purified and cDNA was synthesized. Sequencing libraries were generated using NEB Next® Ultra RNA Library Prep Kit for Illumina® (NEB, USA) following the manufacturer's recommendations. Index codes were added to attribute sequences to each sample. The data were analyzed on the free online platform Majorbio Cloud Platform (www.majorbio.com) of Shanghai Majorbio Bio-pharm Technology Co., Ltd.

Immunofluorescence and Confocal Microscopy

Immunofluorescence and confocal microscopy were performed as described previously [34]. In brief, cryo-sections were incubated with one primary antibody followed by incubation with another primary antibody overnight at 4°C. The same sections were then incubated with the appropriate secondary antibodies. The following primary antibodies were used: mouse anti-GFAP mAb (1:1,000; Sigma-Aldrich, St. Louis, USA) and rabbit anti-IBA1 pAb (1:1,000; WAKO). The following secondary antibodies were used: Alexa Fluor 555 goat anti-mouse IgG (Invitrogen, A-21422), Alexa Fluor 488 goat anti-rabbit IgG (Invitrogen, A27034), and goat anti-rabbit IgG biotin (Invitrogen).

Western Blot Analysis and Quantification

Western blotting was performed as described previously [29]. The following primary antibodies were used: mouse anti-GAPDH mAb (1:5000; SAB, China. 1336), mouse anti-β-actin mAb (1:5000; Sigma-Aldrich, USA. A5441),

and rabbit anti-DRD2 (1:1000, Frontier Institute Co. Ltd. Japan. AB_2571596). The membrane was washed and incubated for 1 h at room temperature with the corresponding secondary antibodies: horseradish peroxidase (HRP)-conjugated goat anti-rabbit IgG (1:10,000; Jackson ImmunoResearch Laboratories, West Grove, PA, USA, 111–035–003), and HRP-conjugated goat anti-mouse IgG (1:10,000; Jackson ImmunoResearch Laboratories, 115–035–003). Peroxidase activity was detected with the SuperSignal WestPico chemiluminescent substrate (Pierce Biotechnology) and visualized and digitized with ImageQuant (LAS-4000, Fujifilm, Japan). Optical densities of bands were analyzed using ImageJ software (NIH, USA). Protein levels, quantified by computer analysis as the ratio between each the immunoreactive band and the β-actin band, are expressed as a percentage of vehicle-treated control.

Dopamine Measurement Using HPLC

Fecal sample preparation and colonic free active DA measurement were as described previously [24]. Briefly, mice aged 2, 12, or 18 months were anesthetized with 10μL/g of body weight 30% ethyl carbamate and sacrificed by cervical dislocation. The lumen contents were weighed and homogenized in 0.01 mol/L ice-cold PBS. The supernatant was collected by centrifugation followed by incubation with aluminum oxide. DA was eluted from the aluminum oxide and the supernatant was processed for DA measurement by an HPLC system (Thermo UltiMate 3000 with an electrochemical detector, Coulochem III, and Agilent Eclipse Plus C18 column). For striatal DA measurement, samples were prepared as described previously [31]. Briefly, striatal tissue was homogenized in 0.2 mol/L perchloric acid by vortexing. The supernatant was collected by centrifugation for 30 min at 12,000 g and processed for DA measurement by the HPLC system

CCK8 Assay and JC-1 Assay

The cell counting 8 (CCK8) assay was carried out to assess cell proliferation according to the manufacturer's instructions (Beyotime Biotechnology, China), Briefly, SH-SY5Y human neuroblastoma cells (ATCC CRL-2266) were maintained in DMEM with 10% fetal bovine serum at 37°C under 5% CO_2. Cells were seeded on a 96-well plate 24 h before treatment. Cells were exposed to 10 or 20 mmol/L succinate for 6 h followed by incubation with 2 mmol/L MPP^+ (Sigma-Aldrich, D048) for 24 h. The absorbance was measured at 450 nm using a microplate reader after 2 h incubation with CCK8 solution.

The mitochondrial membrane potential was measured in SH-SY5Y cells following succinate and MPP^+ treatment using the JC-1 kit (Beyotime Biotechnology, China) according to the manufacturer's instructions. The membrane potential was calculated as the ratio of red/green fluorescent signal intensity.

RNA Isolation and Quantitative PCR

Total RNA was isolated using TRIzol reagent (Invitrogen, USA) and subjected to cDNA synthesis. qPCR was performed by using TBGreen Supermix (Roche, USA). Primers were designed using the Primer Picking Program and their sequences were as follows: β-actin (Actb), forward, 5′-GAGATTACTGCCCTGGCTCCTA-3′, reverse, 5′-TCATCGTACTCCTGCTTGCTGAT-3′. Drd1, forward, 5′-TCTCCCAGATCGGGCATTTG-3′, reverse, 5′-AAGGACCCAAAGGGCCAAAA-3′. Drd2, forward, 5′-AAACACCAGGTAGCTCCACG-3′, reverse, 5′-CCG AAGGGTACAGAAACCCC-3′. Drd3, forward, 5′-AGC ATCCTGAACCTCTGTGC-3′, reverse, 5′-ACTGGCT GTTCTGTCGAGTG-3′. Drd4, forward, 5′-TTGGTGTT GGCAGGGAACTC-3′, reverse, 5′-ACTGACCCTGCTG GTTGTAG-3′. Drd5, forward, 5′-AGATCGCTGCTGCC-TATGTC-3′, reverse, 5′-CAAAGCAAAGGTGACTGC CC-3′. Pink1, forward, 5′-CTTGCCCCACACCCTAAC AT-3′, reverse, 5′-TGAGTCCCACTCCACAAGGA-CAT GCCTACATTGCCCCAGA 3′. Parkin, forward, 5′-CC GAATCACCTGACGGTTCA-3′, reverse, 5′-GAGGGT TGCTTGTTTGCAGG -3′. Atg5, forward, 5′-ATTAGCA TTGTCCCCCAGCC-3′, reverse, 5′-TCTTCTCCTCC TTGGCTTGC-3′. Bcl2, forward, 5′-TCTTTTCGGGGAA GGATGGC-3′, reverse, 5′-GACGGTAGCGACGAGAGA AG-3′. Bax, forward, 5′-CTCCGGCGAATTGGAGAT GA-3′, reverse, 5′-GAGGAAGTCCAGTGTCCAGC-3′. HIF-1α, forward, 5′-GGCAGCGATGACACAGAAAC-3′, reverse, 5′-GGGACTGTTAGGCTGGGAAA-3′. PLCG2, forward, 5′-CAGCTTCCCCGTCATCTTGT-3′, reverse, 5′-TGTCATCACCGAAGGACAGC-3′.IL-1β, forward, 5′-TGCCACCTTTTGACAGTGATG-3′, reverse, 5′-AAG GTCCACGGGAAAGACAC-3′. IL-6, forward, 5′-TTGGG ACTGATGCTGGTGAC-3′, reverse, 5′-TGTGACTCCA GCTTATCTCTTGG-3′. Muc2, forward, 5′-ACCTCCA GGTTCAACACCAG-3′, reverse, 5′-ATGGCAGTCCA-GAGAGCAGT-3′. Homo Atg5, forward, 5′-GTAGTT GCCTGGAGGAGCG-3′, reverse, 5′-CATGTACCCCAA-GAGGGACC-3′. Homo Pink1, forward, 5′-CATGCCTA-CATTGCCCCAGA-3′, reverse, 5′-TGACTGCTCCATA CTCCCCA-3′. Homo Parkin, forward, 5′-GCTCAAG-GAGGTGGTTGCTA-3′, reverse, 5′-AGTGTGCAGAAT-GACAGCCA-3′. Homo Bcl2, forward, 5′-ACCATGG

CGCACGCTGGGAGAACGGGGTAC-3′, reverse, 5′-CTTGTGGCTCAGATAGGCACC-3′. Homo Bax, forward, 5′-ACCATGGACGGGTCCGGGGAGCAGCCCAGA-3′, reverse, 5′-GCCCATCTTCTTCCAGATGGTTGA-3′.

Stool DNA Extraction and Quantitative PCR

Stool DNA was extracted using the QIAamp Fast DNA Stool Mini Kit according to the manufacturer's instructions. The primer design was based on the literature [35] and their sequences were as follow: Total bacteria, forward 5′-GGTGAATACGTTCCCGG-3′, reverse, 5′-TACGGCTACCTTGTTACGACTT-3′. *Prevotella*, forward, 5′-GGGAGGCAGCAGTGAGGAAT-3′, reverse, 5′-CTGGCACGGAATTAGCCGGT-3′. *Alloprevotella*, forward, 5′-CGAGTTGTCCAGCGAAAGCG-3′, reverse, 5′-CTGCACTCCGCACTCTTGGT-3′.

Statistical Analysis

Statistical analysis was applied using GraphPad software (GraphPad Prism v7.0; GraphPad Software, USA). Data presented as mean ± SEM were submitted to two-sided one-/two-way ANOVA followed by either the Dunnet test or Student–Newman–Keul's test (as a *post hoc* test). $P < 0.05$ was considered significant. In each experiment, appropriate positive and negative controls were set up and used to make a judgment on whether the data were excluded or not. This is reflected in many of the figures.

Results

Colonic Dopamine Signaling Is Reduced in Aged Mice

To identify changes in the intestinal DAergic system during ageing, we compared global transcriptional expression profiles in large IECs (LIECs) between young (2 months old) and aged mice (18 months old) (Fig. 1A) using RNA-sequencing (RNA-seq). Analysis of differentially-expressed genes (DEGs) between young and aged mice showed 151 upregulated and 1,476 downregulated genes (with >2-fold changes and $P < 0.05$) (Fig. 1B). Using unsupervised clustering analysis, we examined the expression profiles of the DEGs associated with DA signaling between the genotypes. This showed a marked downregulation of genes associated with DA signaling, including Arrb2, Gria3, and Gria4, which are components of classical DRD2 signaling [36], in aged colon tissue compared to the young counterparts (Fig. 1C, D). Gria3 encodes GluA3, which is required to maintain normal DA levels in the striatum [36]. Gnb4, Gng2, and Gng11 encode Gi/0 and are essential for DA signaling. Among these downregulated genes, the expression levels of Cryab, which encodes αB-crystallin and is a non-canonical downstream signaling target of DRD2 preferentially in astrocytes [29, 37, 38], was also significantly reduced in older mice (Fig. 1E), suggesting a significant impairment in both canonical and non-canonical DRD2 signaling in the aged gut. In support of this, we found a trend towards a decrease in the expression levels of both DRD2 protein and Drd2 mRNA in LIECs of aged mice as compared with young animals (Fig. 1H–J). Moreover, the free active DA levels in the colonic lumen of aged mice were significantly lower than in young mice, as measured by HPLC (Fig. 1F). Together, these results suggest that DRD2 signaling in the large intestine of mice is suppressed during ageing.

Mesencephalic DA Neurons of Drd2vil1 Mice Are More Vulnerable to MPTP-induced Neurotoxicity

To assess the impact of altering intestinal DRD2 on nigral DA neurons in the brain, we generated *Drd2* conditional knockout (cKO) mice, in which *Drd2* was ablated selectively in IECs, by crossing *Drd2*-floxed mice with villin 1 (Vil1)-Cre transgenic (Tg) mice. Removal of *Drd2* from Vil1-Cre mice was highly efficient (Fig. 2A), as there was a marked reduction of Drd2 mRNA in the LIECs of $Drd2^{vil1}$-cKO mice compared to wild-type animals (Fig. 2A, B). Ablation of *Drd2* in the intestinal epithelium was also DA receptor subtype-specific, as the expression of other DA receptor family members, such as Drd1 and Drd3–5, was not significantly altered (Fig. 2A, B), when assessed by real-time PCR. Interestingly, this genetic manipulation only affected DRD2 expression in epithelial cells of the large intestine, but not the small intestine. Furthermore, selective ablation of *Drd2* in the intestine also showed tissue or organ-specificity, as the expression of DRD2 in the striatum, where *Drd2* is highly enriched in the brain, was not significantly perturbed (Fig. 2C).

Next, we investigated the response of $Drd2^{vil1}$-cKO mice to neurotoxicity induced by MPTP, a well-known neurotoxicant inducer of parkinsonism. We used an acute intoxication paradigm (Fig. 2D) that induces both motor and non-motor symptoms in rodents [30]. Besides, manipulation of gut microbiota by broad-spectrum antibiotics rescues the neuronal loss in the acute MPTP mouse model [39]. We found that $Drd2^{vil1}$-cKO mice were more sensitive to MPTP challenge, exhibiting more TH^+ neuron loss in the SN than in MPTP-treated WT counterparts (Fig. 2E, F). Consistent with this, ablation of *Drd2* in the intestinal epithelium exacerbated the MPTP-induced reduction in striatal DA levels (Fig. 2G). Comparatively more activated ionized Ca^{2+}-binding adaptor molecule 1 (Iba1)-positive microglia, but not glial fibrillary acidic

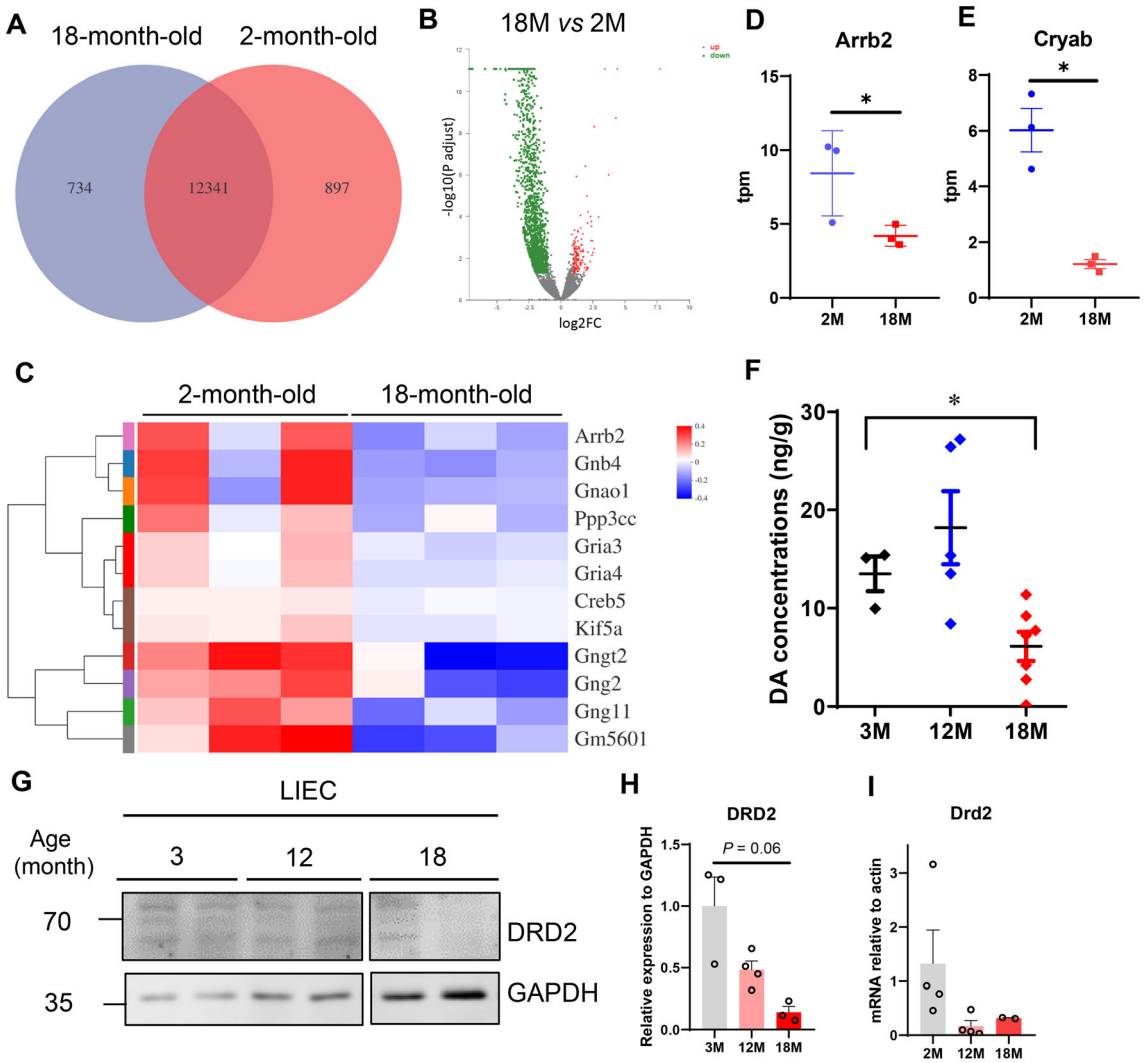

Fig. 1 Reduced expression of dopamine signaling-associated genes and dopamine levels in large intestine of aged mice. **A** Venn plot of detected genes in large intestinal epithelial cells analyzed by RNA-seq in 2-month-old (2M) and 18-month-old (18M) mice. **B** A volcano plot showing the up- and down-regulated genes in 2M and 18M mice. **C** A heatmap showing downregulated expression of genes associated with DA signaling in large intestinal epithelial cells of 2M or 18M mice. **D, E** Expression of *Arrb2* and *Cryab* in RNA-seq analysis is significantly decreased in 18M mice. Data are presented as the mean ± SEM, $n = 3$. Unpaired *t*-test. *$P < 0.05$. **F** Concentrations of free active DA in the colonic lumen measured by HPLC. Data are presented as the mean ± SEM, 3-month-old (3M), $n = 3$; 12-month-old (12M), $n = 5$, 18-month-old (18M), $n = 7$. One-way ANOVA followed by *post-hoc* test. *$P < 0.05$. **G–I** Expression of DRD2 in large intestinal cells assessed in 3M, 12M, and 18M mice. The intestinal epithelial DRD2 levels are assessed by western blotting (**G**), and quantitative data are shown in (**H**). Data are presented as the mean ± SEM, 3M, $n = 3$; 12M, $n = 4$, 18M, $n = 3$. One-way ANOVA followed by *post-hoc* test. *$P < 0.05$. **I** Levels of Drd2 mRNA in the intestinal epithelium of mice assessed by quantitative PCR at various ages. Data are presented as the mean ± SEM, 3M, $n = 4$, 12M, $n = 4$, 18M, $n = 2$. Unpaired *t*-test. *$P < 0.05$.

protein (GFAP)-positive astrocytes were observed in the substantia nigra pars compacta (SNc) of *Drd2*^{vil1} cKO mice (Fig. 2H, I). These data indicate that the absence of *Drd2* in the intestinal epithelium sensitizes the evoked nigral DA neuron degeneration in a cross-organ manner.

Considering the relatively similar biological responses among three members of the D2-like receptor subfamily (DRD2–4) and DRD4 is relatively highly abundant in the intestinal epithelium [40], we determined whether intestinal epithelial *Drd4* is involved in the regulation of nigral DA neuron survival. We generated *Drd4*-cKO mice by breeding *Drd4*-floxed mice with *Vil1-Cre* Tg mice. Seven days following administration of MPTP, there was no significant loss in the number of TH$^+$ cells in the SN of *Drd4*^{vil1}-cKO mice than in WT controls. Likewise, no significant difference in striatal DA levels between genotypes was found (Fig. 2J–L). Together, these results suggest that DRD2 in the intestinal epithelium is required

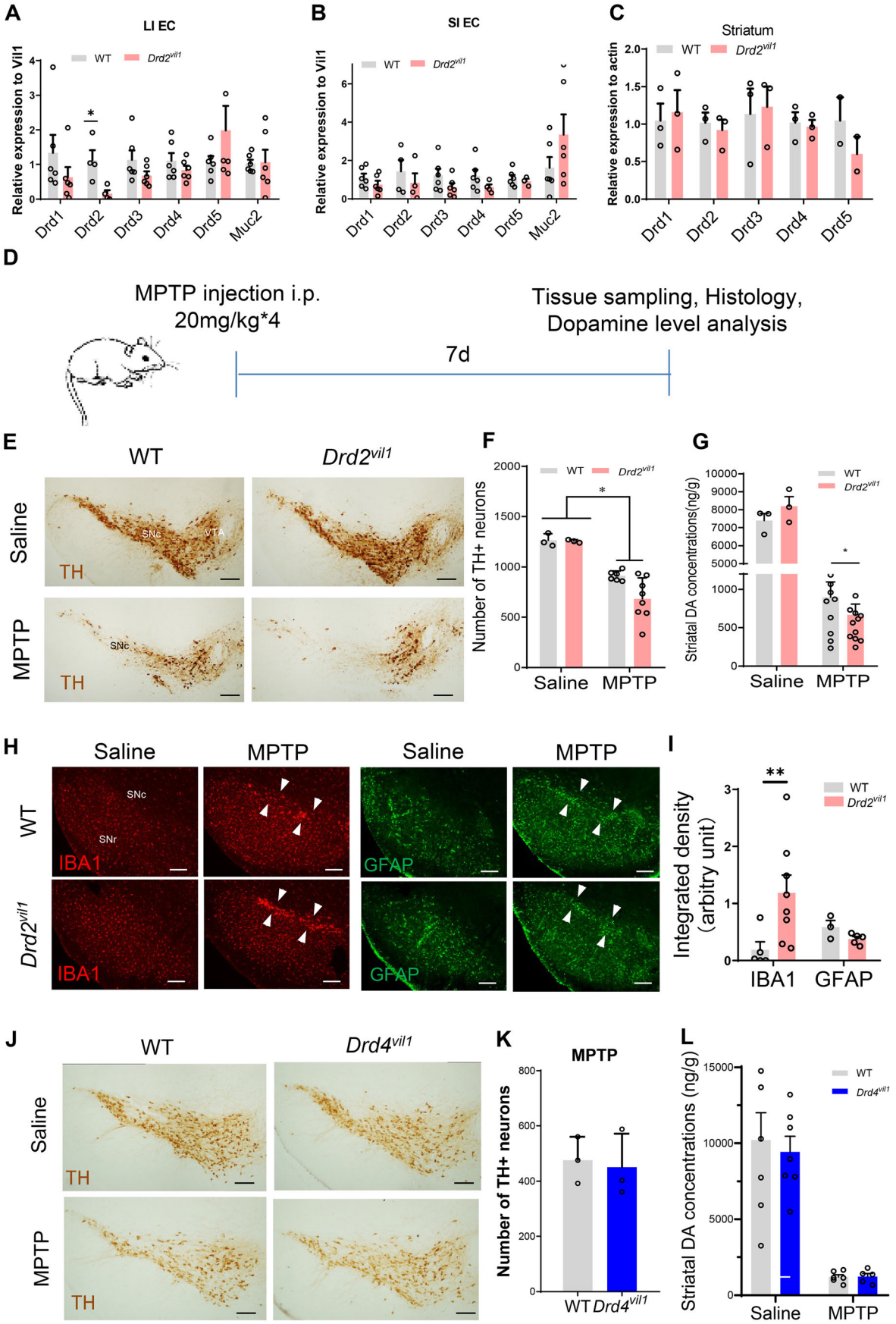
A
LI EC
WT
Drd2vil1
Relative expression to Vil1
Drd1
Drd2
Drd3
Drd4
Drd5
Muc2
B
SI EC
C
Striatum
Relative expression to actin
D
MPTP injection i.p.
20mg/kg*4
7d
Tissue sampling, Histology,
Dopamine level analysis
E
Saline
MPTP
SNc
VTA
TH
F
Number of TH+ neurons
G
Striatal DA concentrations(ng/g)
H
SNr
IBA1
GFAP
I
Integrated density
(arbitry unit)
J
Drd4vil1
K
MPTP
L

◀**Fig. 2** *Drd2*^{vil1} mice display enhanced vulnerability of mesencephalic dopaminergic neurons to MPTP-induced neurotoxicity. **A–C** Representative graphs showing the efficacy of *Drd2* knockdown in large intestinal epithelial cells (LIECs) (**A**), $n = 6$, small intestinal epithelial cells (SIECs) (**B**), $n = 6$, or striatum (**C**) of *Drd2*^{vil1} mice. $n = 3$. **D** Schematic showing the timeline of acute MPTP treatment. **E** Representative microphotographs showing the survival of nigral TH$^+$ cells in *Drd2*^{vil1}-cKO mice exposed to MPTP or saline. SNc, substantia nigra pars compacta; VTA, ventral tegmental area. **F** Quantitative data of (**E**). **G** Measurement of striatal dopamine levels in *Drd2*^{vil1}-cKO mice and control animals after MPTP challenge. Saline, $n = 3$. MPTP + WT, $n = 9$. MPTP+ *Drd2*^{vil1}-cKO, $n = 12$. All data are presented as the mean ± SEM, Unpaired *t*-test. *$P < 0.05$, **$P < 0.01$. **H**, **I** Immunohistochemical analysis of *Drd2*^{vil1}-cKO and control mice; ventral mesencephalic sections were taken 7 days after challenge with MPTP. SNr, substantia nigra pars reticulata. Arrowheads indicate the glia scar in the SNc. Scale bars, 400 μm. Quantitative data of (**H**) are shown in (**I**). **J** Immunohistochemical analysis of ventral mesencephalic sections taken after 7 days from *Drd4*^{vil1}-cKO mice that received MPTP. **K** Quantitative data of (**J**). WT + MPTP, $n = 3$, *Drd4*^{vil1}-cKO + MPTP, $n = 3$. **L** Striatal DA levels measured using HPLC in *Drd4*^{vil1}-cKO mice and controls 7 days after MPTP administration. WT + saline, $n = 7$; *Drd4*^{vil1}-cKO + Saline, $n = 6$, *Drd4*^{vil1}-cKO + MPTP, $n = 5$. All data are presented as the mean ± SEM, unpaired *t*-test.

for maintaining the normal function of DA neurons in the MPTP-induced PD model.

Reduced Abundance of Alleoprevotella in Drd2vil1-cKO Mice Following MPTP Exposure

Given that the gut microbiota is the major source of intestinal DA [24] and levels of colonic free active DA decreased with ageing (Fig. 1), we speculated that there is dysbiosis in the gut microbiota during ageing. Whether deregulated intestinal epithelial DRD2 contributes to this process is uncertain. We thus investigated whether the disruption of DRD2 signaling in the intestinal epithelium perturbs microbe composition and its metabolism contributes to the increased vulnerability to MPTP-induced neurotoxicity. We analyzed the gut microbiota composition of 2-month-old WT or *Drd2*^{vil1}-cKO mice exposed to either MPTP or vehicle, using 16S ribosomal RNA sequencing. A total of 66 operational taxonomic units (OTUs) were detected as core microbiota in a Venn diagram of intestinal microbiota (Fig. 3A). Of these, *Bacteroidetes* was one of the predominant bacteria at the genus level across the four groups (Fig. 3B). We found that, following the MPTP challenge, the genus *Faecalibaculum* was almost excluded in both WT and *Drd2*^{vil1}-cKO mice among the 15 most abundant genera, as compared to saline-treated animals (Fig. 3A–C). Notably, the abundance of some bacteria that have been reported to be decreased in PD patients [22] [41] was also lower in *Drd2*^{vil1}-cKO mice than in WT mice after MPTP challenge. These genera included *Blautia* (5%), *Prevotellaceae* (7%), and *Faecalibacterium* (30%) (Fig. 3D, E). In contrast, the abundance of some pathogenic intestinal bacteria was increased, and these genera included *Lactobacillus* (10%) and *Akkermansia* (5%) in the *Drd2*^{vil1}-cKO/MPTP group. Besides, the relative abundance of the genus *Alloprevotella* (5%) was significantly different between groups (Fig. 3D, E) [40]. These results suggest that *Drd2* deficiency together with MPTP treatment profoundly changes the intestinal microbiota composition and results in a compromised gut microbiota-mediated neuroprotective activity.

Previous studies have indicated that *Alleoprevotella* is strongly associated with PD. The abundance of *Prevotella* is significantly decreased in PD patients, and *Prevotella*-derived hydrogen sulfide is neuroprotective in PD [42–44]. It is known that *Alleoprevotella* belongs to the family *Provotellaceae* and is evolutionarily close to the genus *Prevotella* [45]. *Alleoprevotella* uses dietary fibers to produce acetic acid and succinic acid [45]. Besides, there is evidence that the fecal concentration of succinic acid is significantly lower in patients with PD relative to control subjects [46]. These data indicate that *Alleoprevotella* and fecal succinic acid play a role in PD pathogenesis.

As shown in Fig. 3, the altered microbiome in *Drd2*^{vil1}-cKO mice may be attributable to the perturbed secretory activity of IECs, as they play an important role in regulating the gut microbiota [47, 48]. We thus examined whether selective ablation of *Drd2* in intestinal epithelium changes the function of goblet cells. We found no significant change in the number of goblet cells in both the large and small intestines of *Drd2*-deficient mice as compared to controls (Fig. 4A–C). There was also no significant difference in Periodic acid-Schiff staining (Fig. 4A), indicating that *Drd2* deficiency does not have a profound impact on acetic mucin secretion by LIECs. This result was consistent with the finding that there was no significant alteration in expression levels of mucin2 mRNA in both LIECs and small IECs between genotypes (Fig. 2A, B). Moreover, no marked change in the colon length and inflammatory factor mRNA expression was found between genotypes, indicating that no inflammatory response is involved in *Drd2*^{Vil1}-cKO mice (Fig. 4D, E). Together, these data suggest that the intestinal epithelial cell barrier is not involved in the increased vulnerability of nigral DA neurons in *Drd2*^{vil1}-cKO mice following exposure to MPTP.

Intestinal Epithelial Drd2 Controls the Transcriptional Expression of Mitochondria-related Gene Sets in the Brain

To understand how intestinal *Drd2* deficiency-induced gut microbiome alteration regulates brain activity, we then

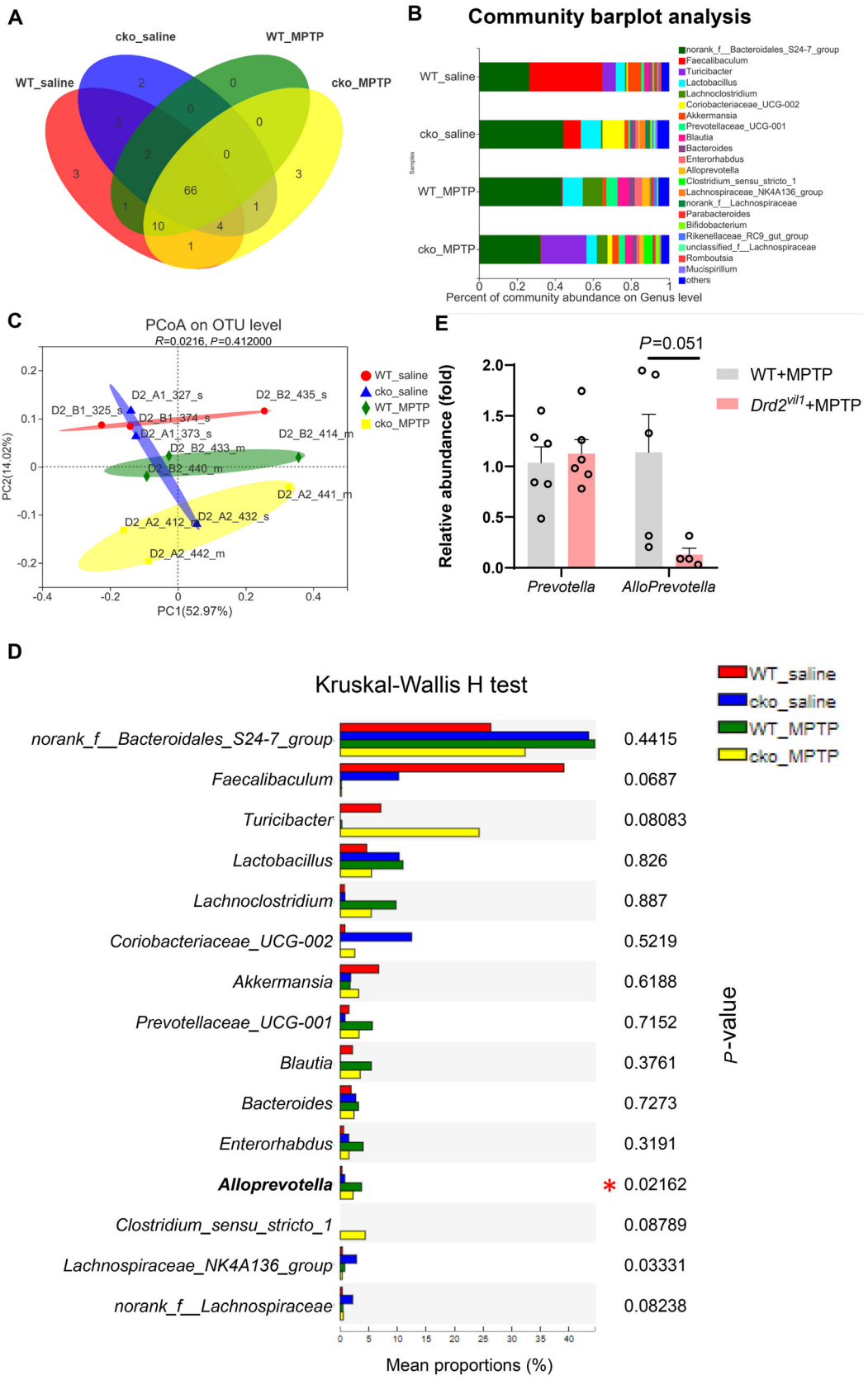
A
cko_saline
WT_MPTP
WT_saline
cko_MPTP
B
Community barplot analysis
WT_saline
cko_saline
WT_MPTP
cko_MPTP
Samples
norank_f__Bacteroidales_S24-7_group
Faecalibaculum
Turicibacter
Lactobacillus
Lachnoclostridium
Coriobacteriaceae_UCG-002
Akkermansia
Prevotellaceae_UCG-001
Blautia
Bacteroides
Enterorhabdus
Alloprevotella
Clostridium_sensu_stricto_1
Lachnospiraceae_NK4A136_group
norank_f__Lachnospiraceae
Parabacteroides
Bifidobacterium
Rikenellaceae_RC9_gut_group
unclassified_f__Lachnospiraceae
Romboutsia
Mucispirillum
others
Percent of community abundance on Genus level
C
PCoA on OTU level
R=0.0216, P=0.412000
WT_saline
cko_saline
WT_MPTP
cko_MPTP
D2_A1_327_s
D2_B2_435_s
D2_B1_325_s
D2_B1_374_s
D2_A1_373_s
D2_B2_414_m
D2_B2_433_m
D2_B2_440_m
D2_A2_441_m
D2_A2_412_s
D2_A2_432_s
D2_A2_442_m
PC2(14.02%)
PC1(52.97%)
E
P=0.051
WT+MPTP
Drd2vil1+MPTP
Relative abundance (fold)
Prevotella
AlloPrevotella
D
Kruskal-Wallis H test
WT_saline
cko_saline
WT_MPTP
cko_MPTP
norank_f__Bacteroidales_S24-7_group 0.4415
Faecalibaculum 0.0687
Turicibacter 0.08083
Lactobacillus 0.826
Lachnoclostridium 0.887
Coriobacteriaceae_UCG-002 0.5219
Akkermansia 0.6188
Prevotellaceae_UCG-001 0.7152
Blautia 0.3761
Bacteroides 0.7273
Enterorhabdus 0.3191
Alloprevotella * 0.02162
Clostridium_sensu_stricto_1 0.08789
Lachnospiraceae_NK4A136_group 0.03331
norank_f__Lachnospiraceae 0.08238
P-value
Mean proportions (%)

◀**Fig. 3** Reduced abundance of succinate-producing *Alleoprevotella* in the intestine of *Drd2*^{vil1}-cKO mice following MPTP exposure. **A** Venn diagram depicting unique and shared operational taxonomic units (OTUs) among different groups. **B** Percent of community abundance at the genus level based on bacterial community barplot analysis. Data are present as the mean, n = 3. **C** Beta-diversity analysis presented as a two-dimensional plot based on principal coordinate analysis (PCoA), UniFrac weighted (P = 0.2930, R = 0.0864). **D** Multi-group comparison analysis based on the Kruskal-Wallis H test showing that the relative abundance of *Alleoprevotella* is significantly different among groups. Data are presented as the mean, n = 3, Kruskal-Wallis H test, *P <0.05. **E** qPCR analysis of fecal pellets showing relative abundance of *Prevotella* and *Alleoprevotella* in MPTP-challenged WT and *Drd2*^{vil1}-cKO mice. WT + MPTP, n = 5, *Drd2*^{vil1}-cKO + MPTP, n = 4. Data are presented as the mean ± SEM, unpaired t-test. *P <0.05.

analyzed the transcriptome of the SN of *Drd2*^{vil1}-cKO mice *via* bulk RNA sequencing. This revealed 2,038 upregulated genes and 1,618 downregulated genes among 3,656 total DEGs between genotypes (Fig. 5A, B). GO enrichment analysis showed that large numbers of DEGs were highly enriched in mitochondrial function-related pathways (Fig. 5C). Among these DEGs, the expression levels of Pink1 and Atp5e, regulators of mitophagy, as well as Bax, a core regulator of the intrinsic pathway of apoptosis, were significantly elevated in *Drd2*^{vil1}-cKO mice (Fig. 5C), indicating deregulated mitochondrial activity in the SN of *Drd2*^{vil1}-cKO mice. Next, we validated the RNA-seq data in the SN of mice exposed to MPTP using qPCR. Consistent with the data shown in Fig. 5E, there was a pronounced increase in mRNA levels of Atg5 and a trend toward an increase in levels of Pink1, Parkin, and Bax in the SN of *Drd2*^{vil1}-mice after MPTP injection (Fig. 5F). Taken together, our data suggest that intestinal DRD2 plays a key role in the regulation of mitochondrial dynamics and function in the brain.

Administration of Succinate Markedly Attenuates the Dopaminergic Neuronal Loss Induced by MPTP

Given that intestinal DRD2 has been shown to be required for the maintenance of succinate-producing *Alleoprevotella* in the gut as well as the regulation of mitochondrial function in the brain, we speculated that fecal succinate may influence mitochondrial activity in the brain, providing a molecular basis for intestinal DRD2-dependent neuroprotection. To test this speculation, we first examined the effect of succinate on the survival of SH-SY5Y human neuroblastoma cells exposed to MPP^+, an active metabolite of the neurotoxin MPTP, for 24 h (Fig. 5G). Pretreatment of SH-SY5Y cells with succinate significantly rescued MPP^+-induced cell death as assessed by CCK8 staining (Fig. 5H). In living organisms, succinate is known to be converted into fumarate by the enzyme succinate dehydrogenase in complex II of the electron transport chain that is involved in the production of ATP in mitochondria [49]. It is well known that MPP^+ inhibits electron transport chain complex I [4]. We thus investigated whether treatment with succinate can stabilize mitochondrial function, contributing to neuroprotection. As expected, pretreatment of SH-SY5Y cells with succinate dramatically protected the mitochondria from MPP^+-induced damage at different doses, as assessed by measurement of the mitochondrial membrane potential (MMP) (Fig. 5I, J).

Moreover, we investigated whether succinate has such effects in the MPTP-induced PD model *in vivo*. WT mice were administered succinate for 5 consecutive days followed by intraperitoneal injection of MPTP (Fig. 6A). We found that succinate treatment markedly protected WT mice from MPTP-induced neurotoxicity, as evidenced by an increase in the number of TH^+ neurons in the SN and elevated striatal DA levels compared to MPTP alone (Fig. 6B–E).

Furthermore, we investigated whether the increased vulnerability of nigral DA neurons in *Drd2*^{vil1}-cKO mice to MPTP-induced neurotoxicity can be rescued by succinate treatment. *Drd2*^{vil1} mice were given succinate prior to MPTP administration using the protocol described in Fig. 6A. We found that following pretreatment with succinate, there were higher striatal DA levels compared to control (Fig. 6G). This was accompanied by profoundly reduced activation of Iba1+ microglia in the SNc, indicative of suppressed glial scarring (Fig. 6 H–K), albeit the number of TH^+ neurons in the SN was not successfully restored (Fig. 6F), suggesting that the production of DA in nigral DA neurons of *Drd2*^{vil1} mice is functionally augmented by succinate treatment in an MPTP-induced mouse model. Taken together, these data suggest that loss of fecal succinate contributes to the increased vulnerability of nigral DA neurons in *Drd2*^{vil1}-cKO mice to MPTP-induced neurotoxicity.

Discussion

A number of studies have revealed that the survival and protection of nigral DA neurons against pathological stimuli are influenced by multiple factors primarily derived from the brain. However, little is known about how these processes are regulated *in vivo* by the peripheral tissues/organs and the functional contribution of these mechanisms to the maintenance of nigral DA neuron integrity during neurodegeneration. In the present study, we found that selective *Drd2*-deficiency in the intestinal epithelium resulted in a reduced abundance of succinate-producing *Alleoprevotella*, leading to increased vulnerability of nigral DA neurons to MPTP-induced neurotoxicity. *Drd2*^{vil1}-cKO

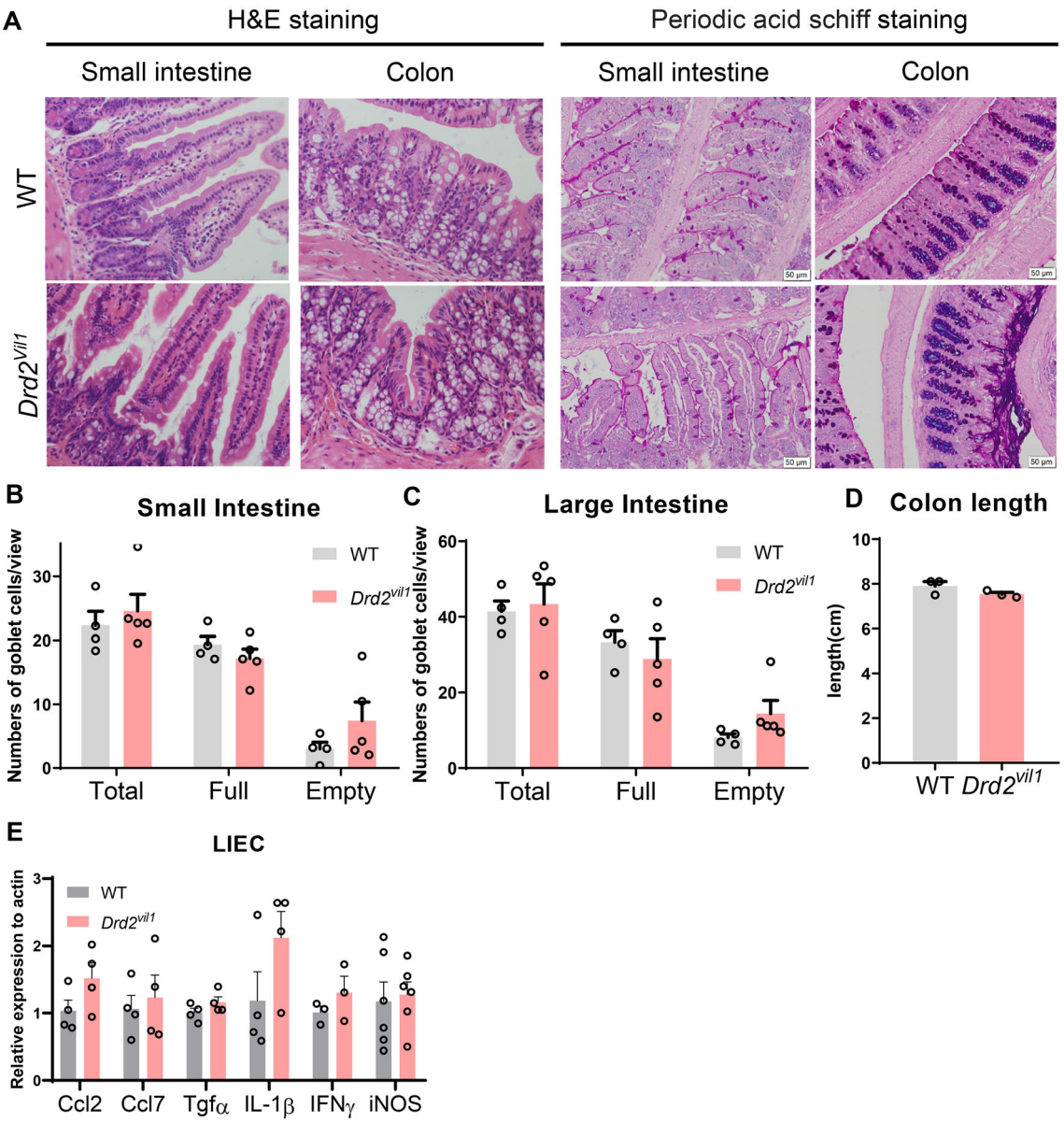

Fig. 4 No alteration in the structure of the intestinal epithelium and goblet function in *Drd2*^{vil1} mice. **A** Histochemical analysis of the small and large intestine epithelium in *Drd2*^{vil1} mice using H&E staining (left panel) and periodic acid Schiff staining (right panel). **B,** **C** Quantitative data as in (**A**). WT (n = 4), *Drd2*^{vil1}-cKO (n = 5). **D** Length of the colon from the cecum to the anus. n = 3. **E** qPCR analysis of inflammatory factors in LIECs. All data are presented as the mean ± SEM, unpaired t-test, n = 6. *P <0.05.

mice displayed aberrant expression of mitochondria-related genes. Moreover, treatment with succinate attenuated the mitochondrial dysfunction and DA neuron loss *in vitro* and in PD animal models. These data suggest that DA/DRD2 signaling in the intestine plays an important role in the maintenance of DA neuron integrity in the brain as well as the protection against pathological stimuli.

The IECs, the very frontline between host and microbiome, provide a robust biochemical and physical barrier to the environment. IECs also serve as an integrative node that receives diverse signals from the gut microbiota, immune cells, and metabolites, modulating a variety of gut activities. Recent studies have suggested that epithelial homeostasis is influenced by ageing and metabolism [50]. However, how the ageing process makes an impact on epithelial homeostasis remains elusive. There is evidence that metabolites have a profound influence on epithelial homeostasis [50]. In the present study, we found that expression of DRD2 in the intestinal epithelium was decreased in aged animals and selective ablation of DRD2

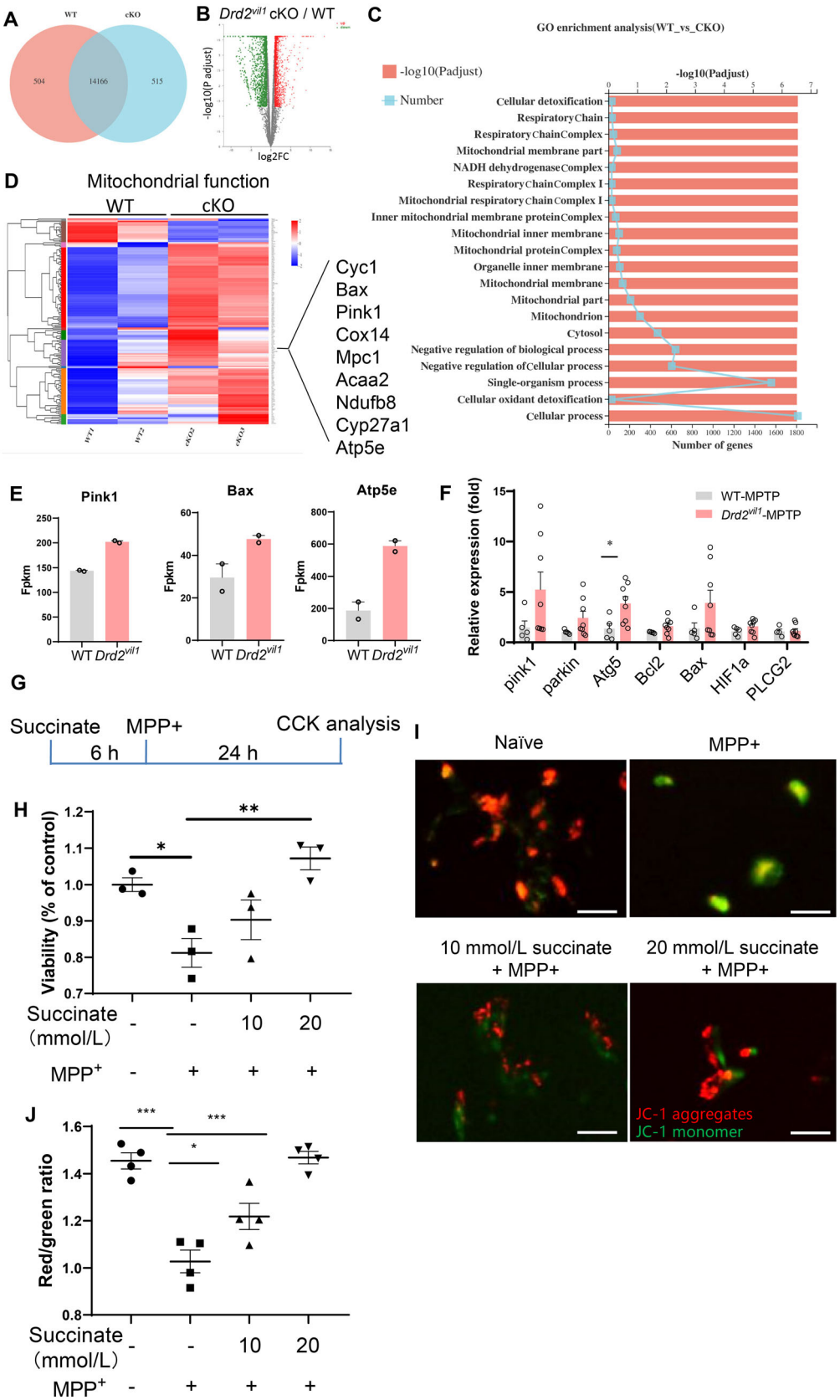
A
WT
cKO
504
14166
515
B
Drd2vil1 cKO / WT
-log10(P adjust)
log2FC
C
GO enrichment analysis(WT_vs_CKO)
-log10(Padjust)
Number
Cellular detoxification
Respiratory Chain
Respiratory Chain Complex
Mitochondrial membrane part
NADH dehydrogenase Complex
Respiratory Chain Complex I
Mitochondrial respiratory Chain Complex I
Inner mitochondrial membrane protein Complex
Mitochondrial inner membrane
Mitochondrial protein Complex
Organelle inner membrane
Mitochondrial membrane
Mitochondrial part
Mitochondrion
Cytosol
Negative regulation of biological process
Negative regulation of Cellular process
Single-organism process
Cellular oxidant detoxification
Cellular process
Number of genes
D
Mitochondrial function
WT
cKO
Cyc1
Bax
Pink1
Cox14
Mpc1
Acaa2
Ndufb8
Cyp27a1
Atp5e
E
Pink1
Bax
Atp5e
Fpkm
WT Drd2vil1
F
WT-MPTP
Drd2vil1-MPTP
Relative expression (fold)
pink1
parkin
Atg5
Bcl2
Bax
HIF1a
PLCG2
G
Succinate
MPP+
CCK analysis
6 h
24 h
H
Viability (% of control)
Succinate (mmol/L)
MPP+
I
Naïve
MPP+
10 mmol/L succinate + MPP+
20 mmol/L succinate + MPP+
JC-1 aggregates
JC-1 monomer
J
Red/green ratio
Succinate (mmol/L)
MPP+

◀**Fig. 5** Succinate pre-treatment attenuates neuronal loss by inhibiting mitophagy both in the SH-SY5Y cell line *in vitro* and $Drd2^{vil1}$ mice *in vivo*. **A** Venn diagram showing the number of differentially expressed genes (FPKM >1) in the SN between WT and $Drd2^{vil1}$-cKO mice. $n = 2$. **B** Volcano plot showing the significantly up- and down-regulated genes between WT and $Drd2^{vil1}$-cKO mice. **C** GO enrichment analysis showing the differentially-expressed genes are highly enriched in mitochondria-related functions. Enrichment is calculated as FPKM. **D** Unsupervised hierarchical clustering of gene expression profiles associated with mitochondrial function. **E** Expression of *Pink1*, *Bax*, and *Atp5e* in RNA-seq analysis is increased in $Drd2^{vil1}$-cKO mice. **F** qPCR analysis of mRNA levels of mitophagy and apoptosis markers in $Drd2^{vil1}$-cKO mice and their littermates. WT mice ($n = 5$), $Drd2^{vil1}$-cKO mice ($n = 8$). **G** Schematic of the timeline of succinate treatment of SH-SY5Y cells. **H** OD450 absorption reveals that 20 mmol/L succinate prevents cell death. The concentration of MPP^+ is 2 mmol/L. $n = 3$. **I** Representative microphotographs showing JC-1 (mitochondrial membrane potential, MMP) staining of SH-SY5Y neuroblastoma cells exposed to MPP^+ (4 mmol/L) Red fluorescence represents JC-1 aggregates and higher MMP, whereas green fluorescence represents JC-1 monomer and lower MMP. Scale bars, 125 μm. **J** Mean grey value of red/green ratio shown in G. $n = 4$. All data are presented as the mean ± SEM, Unpaired *t*-test. $^*P < 0.05$, $^{**}P < 0.01$, $^{***}P < 0.001$.

in the intestinal epithelium promoted marked neuropathological changes in a mouse PD model. These results suggest that intestinal epithelial DRD2 signaling plays a crucial role in the maintenance of epithelial homeostasis not only during ageing but also in ageing-associated neurodegeneration.

Interestingly, our finding that DRD2 signaling is required for the maintenance of epithelial homeostasis suggests that intestinal epithelial DRD2 is functionally distinct from that in other parts of the intestinal tissue, such as the muscle strips that are innervated by the enteric nervous system and are involved in the regulation of intestinal motility [51, 52]. This discrepancy indicates complex and diverse regulatory roles of DAergic signaling in various activities of the intestine. Further studies are needed to investigate the role of the DAergic system in different cell types of the intestine.

Emerging studies have shown that PD patients have an impaired gut barrier and distinct gut microbiota compared to healthy controls [16, 22, 42, 53]. Besides, the gut microbiota even differs in the same patient before and after treatment for PD [21]. It remains to be determined whether changes in the gut microbiota can provoke or prevent PD. A previous study showed that gut microbe transplants from patients with PD promote a-synuclein-mediated motor deficits and brain pathology in a genetic mouse PD model. These detrimental effects appear to be mediated by activated microglia provoked by gut microbiota-derived short-chain fatty acids [54], indicating an augmenting effect of the gut bacteria on neurodegeneration in PD. Consistent with this notion, here we found that the gut microbiota from mice with a deficiency of *Drd2* in the intestinal epithelium also showed changes that favor brain pathology in PD. In comparison to short-chain fatty acids that promote microglia-mediated neuroinflammation in PD pathogenesis, the lack of substances that support the survival of neuronal cells represents a distinct mechanism underlying PD pathogenesis. We found that the relative abundance of succinate-producing *Alleoprevotella* was significantly lower in $Drd2^{vil1}$ mice than in WT mice. This finding is in good agreement with previous reports by others that there is a reduction in levels of succinate in the serum of patients with PD compared to healthy controls [55, 56], demonstrating the various ways through which the gut microbiota influence brain activities. Interestingly, a significant increase in the levels of urine succinate is seen in patients with PD and is associated with the severity of motor dysfunction of PD [56], indicating a higher blood clearance rate of succinate in the context of PD, which may lead to a reduction in levels of succinate in the blood and possibly in the brain as well.

A previous study showed that serum succinate is less abundant in older rats than in younger rats [57]. However, the impact of reduction of succinate on the survival of nigral DA neurons under pathological conditions is unknown. We showed here that administration of succinate markedly attenuated DA neuron loss and the glial activation induced by MPTP treatment *in vivo*. Moreover, exogenous succinate facilitates the conversion to fumarate in complex II of the electron transport chain in mitochondria, leading to increased production of ATP thereby maintaining mitochondrial membrane potential after an MPTP challenge. Thus, it is likely that loss of succinate compromises the defense of nigral DA neurons against neurotoxicity, leading to enhanced vulnerability of these neurons during neurodegeneration. Application of metabolites may provide a novel approach for the control of the critical biological response to pathological stimuli, potentially highlighting avenues for the treatment of neurodegenerative diseases such as PD. There remains a need to characterize the effects of gut metabolites on brain activity, particularly under ageing and pathological conditions [58].

In summary, our study demonstrates that the intestinal DA system declines during aging. The perturbed intestinal DA system exacerbates MPTP-induced neuronal loss and glial activation by downregulating the abundance of succinate-producing *Alleoprevotella.* Targeting intestinal epithelial DRD2 and/or administration of succinate may be a new therapeutic strategy for future intervention in PD.

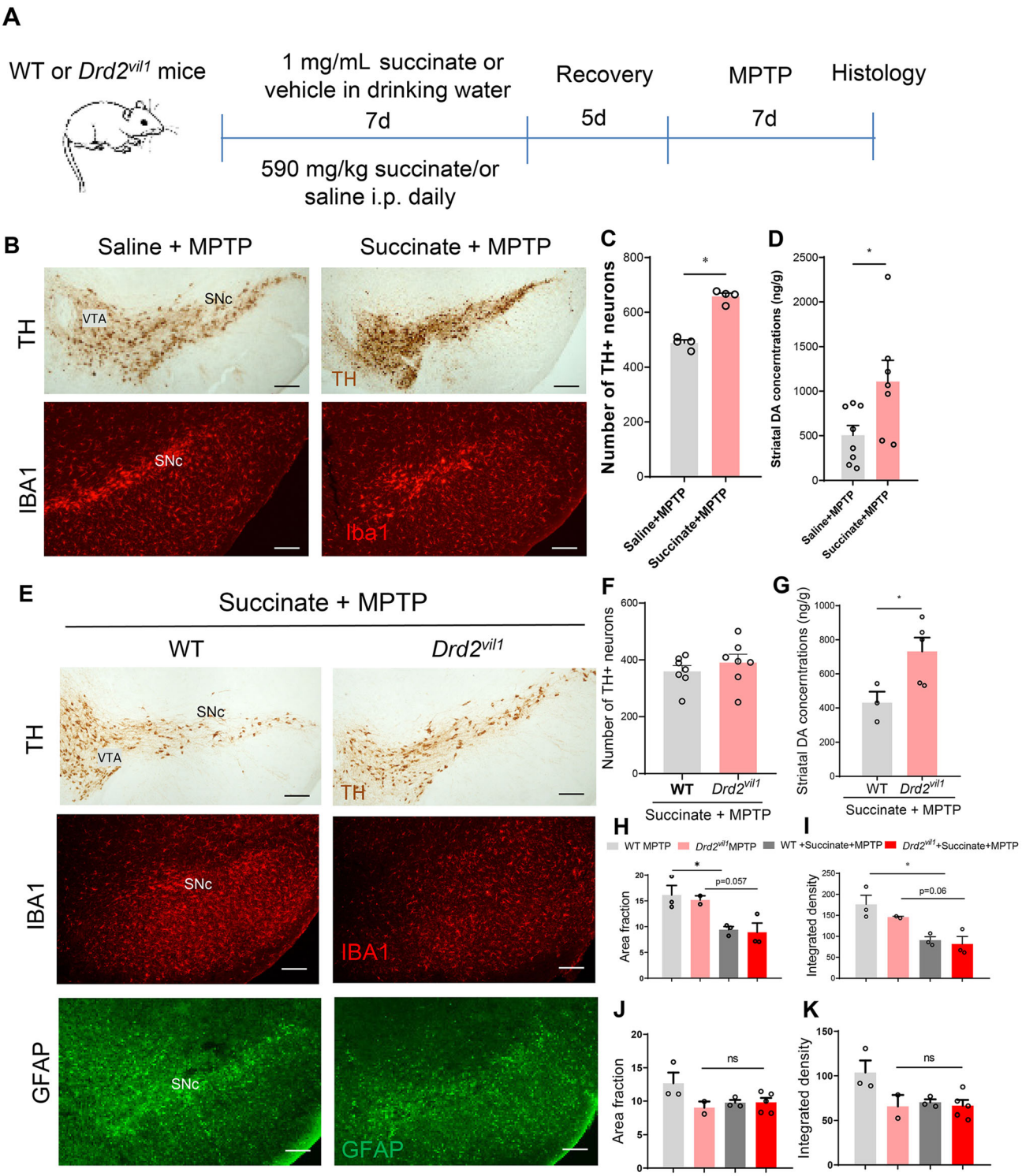

Fig. 6 Administration of succinate markedly attenuates MPTP-induced dopaminergic neuronal loss *in vivo*. **A** Schematic of the timeline of succinate and MPTP treatment of WT mice. **B** Immunohistochemical analysis of TH^+ and $Iba1^+$ cells in ventral mesencephalon sections from WT mice that received repeated succinate and MPTP administration. Scale bars, 400 μm. **C** Quantitative data of (**B**). $n = 4$. **D** Striatal dopamine levels using HPLC in animals subjected to histological analysis in (**B**). Saline + MPTP, $n = 8$, Succinate + MPTP, $n = 7$. **E** Immunohistochemical and immunofluorescence analysis of ventral mesencephalon sections from *Drd2*^{vil1} and control mice that received succinate and MPTP administration. Scale bars, 400 μm. **F** Quantitative data of (**E**), $n = 7$. **G** Striatal dopamine levels from HPLC in animals that were subjected to histological analysis in (**E**). WT mice ($n = 3$), *Drd2*^{vil1}-cKO mice ($n = 5$). **H–K** Quantitative data (**E**) of Iba1 and GFAP immunoreactivity in the SNc. WT + MPTP ($n = 3$), *Drd2*^{vil1}-cKO + MPTP ($n = 2$), WT + succinate + MPTP ($n = 3$), *Drd2*^{vil1}-cKO + succinate + MPTP ($n = 3$). All data are presented as the mean ± SEM, each point represents a mouse. Unpaired *t*-test. $^*P < 0.05$.

Acknowledgements We thank Ms. YQ Yin, YD Li, and JC Hou for excellent technical assistance in animal breeding and genotyping; Dr. Q Hu and his colleagues at the Optical Imaging Center of CEBSIT for technical support in confocal microscopy. This work was supported by grants from the Ministry of Science and Technology of China (2020YFC2002800), the Natural Science Foundation of China (U1801681), Strategic Priority Research Program of Chinese Academy of Science (XDB32020100), Shanghai Municipal Science and Technology Major Project (2018SHZDZX05), Key Realm R&D Program of Guangdong Province (2018B030337001), and Innovative Research Team of High-Level Local Universities in Shanghai.

Conflict of interest The authors declare that they have no competing interests.

References

1. Hou YJ, Dan XL, Babbar M, Wei Y, Hasselbalch SG, Croteau DL, *et al*. Ageing as a risk factor for neurodegenerative disease. Nat Rev Neurol 2019, 15: 565–581.
2. Yamamichi N, Inada KI, Furukawa C, Sakurai K, Tando T, Ishizaka A, *et al*. Cdx2 and the Brm-type SWI/SNF complex cooperatively regulate villin expression in gastrointestinal cells. Exp Cell Res 2009, 315: 1779–1789.
3. O'Toole PW, Jeffery IB. Gut microbiota and aging. Science 2015, 350: 1214–1215.
4. Przedborski S. The two-century journey of Parkinson disease research. Nat Rev Neurosci 2017, 18: 251–259.
5. Kelly CR, Kim AM, Laine L, Wu GD. The AGA's fecal microbiota transplantation national registry: An important step toward understanding risks and benefits of microbiota therapeutics. Gastroenterology 2017, 152: 681–684.
6. Drew L. Two hundred steps. Nature 2016, 538: S2–S3.
7. Travagli RA, Browning KN, Camilleri M. Parkinson disease and the gut: New insights into pathogenesis and clinical relevance. Nat Rev Gastroenterol Hepatol 2020, 17: 673–685.
8. Mukherjee A, Biswas A, Das SK. Gut dysfunction in Parkinson's disease. World J Gastroenterol 2016, 22: 5742–5752.
9. Baek JY, Jeong JY, Kim KI, Won SY, Chung YC, Nam JH, *et al*. Inhibition of microglia-derived oxidative stress by ciliary neurotrophic factor protects dopamine neurons in vivo from MPP^+ neurotoxicity. Int J Mol Sci 2018, 19: E3543.
10. Isaev N, Stelmashook E, Genrikhs EE. Neurogenesis and brain aging. Rev Neurosci 2019, 30: 573–580.
11. Furlan JC, Liu Y, Dietrich WD, Norenberg MD, Fehlings MG. Age as a determinant of inflammatory response and survival of glia and axons after human traumatic spinal cord injury. Exp Neurol 2020, 332: 113401.
12. Boisvert MM, Erikson GA, Shokhirev MN, Allen NJ. The aging astrocyte transcriptome from multiple regions of the mouse brain. Cell Rep 2018, 22: 269–285.
13. Forsyth CB, Shannon KM, Kordower JH, Voigt RM, Shaikh M, Jaglin JA, *et al*. Increased intestinal permeability correlates with sigmoid mucosa alpha-synuclein staining and endotoxin exposure markers in early Parkinson's disease. PLoS One 2011, 6: e28032.
14. Lionnet A, Leclair-Visonneau L, Neunlist M, Murayama S, Takao M, Adler CH, *et al*. Does Parkinson's disease start in the gut? Acta Neuropathol 2018, 135: 1–12.
15. Kim S, Jazwinski SM. The gut microbiota and healthy aging: A mini-review. Gerontology 2018, 64: 513–520.
16. Hill-Burns EM, Debelius JW, Morton JT, Wissemann WT, Lewis MR, Wallen ZD, *et al*. Parkinson's disease and Parkinson's disease medication have distinct signatures of the gut microbiome. Mov Disord 2017, 32: 739–749.
17. Houser MC, Tansey MG. The gut-brain axis: Is intestinal inflammation a silent driver of Parkinson's disease pathogenesis? NPJ Parkinsons Dis 2017, 3: 3.
18. Sun MF, Shen YQ. Dysbiosis of gut microbiota and microbial metabolites in Parkinson's disease. Ageing Res Rev 2018, 45: 53–61.
19. van Kessel SP, Frye AK, El-Gendy AO, Castejon M, Keshavarzian A, van Dijk G, *et al*. Gut bacterial tyrosine decarboxylases restrict levels of levodopa in the treatment of Parkinson's disease. Nat Commun 2019, 10: 310.
20. Keshavarzian A, Engen P, Bonvegna S, Cilia R. The gut microbiome in Parkinson's disease: A culprit or a bystander? Prog Brain Res 2020, 252: 357–450.
21. Bedarf JR, Hildebrand F, Coelho LP, Sunagawa S, Bahram M, Goeser F, *et al*. Functional implications of microbial and viral gut metagenome changes in early stage L-DOPA-naïve Parkinson's disease patients. Genome Med 2017, 9: 39.
22. Keshavarzian A, Green SJ, Engen PA, Voigt RM, Naqib A, Forsyth CB, *et al*. Colonic bacterial composition in Parkinson's disease. Mov Disord 2015, 30: 1351–1360.
23. Wise RA. Dopamine, learning and motivation. Nat Rev Neurosci 2004, 5: 483–494.
24. Asano Y, Hiramoto T, Nishino R, Aiba YJ, Kimura T, Yoshihara K, *et al*. Critical role of gut microbiota in the production of biologically active, free catecholamines in the gut lumen of mice. Am J Physiol Gastrointest Liver Physiol 2012, 303: G1288–G1295.
25. Strandwitz P. Neurotransmitter modulation by the gut microbiota. Brain Res 2018, 1693: 128–133.
26. Chen HW, Nwe PK, Yang Y, Rosen CE, Bielecka AA, Kuchroo M, *et al*. A forward chemical genetic screen reveals gut microbiota metabolites that modulate host physiology. Cell 2019, 177: 1217-1231.e18.
27. Vaiserman AM, Koliada AK, Marotta F. Gut microbiota: A player in aging and a target for anti-aging intervention. Ageing Res Rev 2017, 35: 36–45.
28. Lorente-Picón M, Laguna A. New avenues for Parkinson's disease therapeutics: Disease-modifying strategies based on the gut microbiota. Biomolecules 2021, 11: 433.
29. Shao W, Zhang SZ, Tang M, Zhang XH, Zhou Z, Yin YQ, *et al*. Suppression of neuroinflammation by astrocytic dopamine D2 receptors *via* αB-crystallin. Nature 2013, 494: 90–94.
30. Tieu K. A guide to neurotoxic animal models of Parkinson's disease. Cold Spring Harb Perspect Med 2011, 1: a009316.
31. Jackson-Lewis V, Przedborski S. Protocol for the MPTP mouse model of Parkinson's disease. Nat Protoc 2007, 2: 141–151.
32. Pan D, Das A, Liu D, Veazey RS, Pahar B. Isolation and characterization of intestinal epithelial cells from normal and SIV-infected rhesus macaques. PLoS One 2012, 7: e30247.
33. Zhang SZ, Wang QQ, Yang QQ, Gu HY, Yin YQ, Li YD, *et al*. NG2 glia regulate brain innate immunity *via* TGF-β2/TGFBR2 axis. BMC Med 2019, 17: 204.
34. Cheng XY, Biswas S, Li J, Mao CJ, Chechneva O, Chen J, *et al*. Human iPSCs derived astrocytes rescue rotenone-induced mitochondrial dysfunction and dopaminergic neurodegeneration *in vitro* by donating functional mitochondria. Transl Neurodegener 2020, 9: 13.
35. Hsueh CY, Gong HL, Cong N, Sun J, Lau HC, Guo Y, *et al*. Throat microbial community structure and functional changes in postsurgery laryngeal carcinoma patients. Appl Environ Microbiol 2020, 86: e01849-e11820.
36. Adamczyk A, Mejias R, Takamiya K, Yocum J, Krasnova IN, Calderon J, *et al*. GluA3-deficiency in mice is associated with increased social and aggressive behavior and elevated dopamine in striatum. Behav Brain Res 2012, 229: 265–272.

37. Guo YS, Liang PZ, Lu SZ, Chen R, Yin YQ, Zhou JW. Extracellular αB-crystallin modulates the inflammatory responses. Biochem Biophys Res Commun 2019, 508: 282–288.
38. Lu SZ, Guo YS, Liang PZ, Zhang SZ, Yin S, Yin YQ, *et al*. Suppression of astrocytic autophagy by αB-crystallin contributes to α-synuclein inclusion formation. Transl Neurodegener 2019, 8: 3.
39. Pu Y, Chang L, Qu Y, Wang S, Zhang K, Hashimoto K. Antibiotic-induced microbiome depletion protects against MPTP-induced dopaminergic neurotoxicity in the brain. Aging (Albany NY) 2019, 11: 6915–6929.
40. Zhang XL, Liu SM, Sun Q, Zhu JX. Dopamine receptors in the gastrointestinal tract. Dopamine Gut 2021:53–85.
41. Zhu XL, Li B, Lou PC, Dai TT, Chen Y, Zhuge AX, *et al*. The relationship between the gut microbiome and neurodegenerative diseases. Neurosci Bull 2021, 37: 1510–1522.
42. Mohamed E, Serageldin K, Mohamed K, Koo BB, Schaefer SM. Implications of the gut microbiome in Parkinson's disease. Mov Disord Off J Mov Disord Soc 2020, 35: 921–933.
43. Cakmak YO. Provotella-derived hydrogen sulfide, constipation, and neuroprotection in Parkinson's disease. Mov Disord 2015, 30: 1151.
44. Kida K, Yamada M, Tokuda K, Marutani E, Kakinohana M, Kaneki M, *et al*. Inhaled hydrogen sulfide prevents neurodegeneration and movement disorder in a mouse model of Parkinson's disease. Antioxid Redox Signal 2011, 15: 343–352.
45. Downes J, Dewhirst FE, Tanner ACR, Wade WG. Description of Alloprevotella rava gen. nov., sp. nov., isolated from the human oral cavity, and reclassification of Prevotella tannerae Moore et al. 1994 as Alloprevotella tannerae gen. nov., comb. nov. Int J Syst Evol Microbiol 2013, 63: 1214–1218.
46. Sarah V, Vanessa P, Marta M, Silvia P, Roberto C, Paolo U, *et al*. Gut microbiota and metabolome alterations associated with Parkinson's disease. mSystems 2020, 5: e00520-5e00561.
47. Kurashima Y, Kiyono H. Mucosal ecological network of epithelium and immune cells for gut homeostasis and tissue healing. Annu Rev Immunol 2017, 35: 119–147.
48. Solis AG, Klapholz M, Zhao JR, Levy M. The bidirectional nature of microbiome-epithelial cell interactions. Curr Opin Microbiol 2020, 56: 45–51.
49. Tretter L, Patocs A, Chinopoulos C. Succinate, an intermediate in metabolism, signal transduction, ROS, hypoxia, and tumorigenesis. Biochim Biophys Acta 2016, 1857: 1086–1101.
50. Funk MC, Zhou J, Boutros M. Ageing, metabolism and the intestine. EMBO Rep 2020, 21: e50047.
51. Colucci M, Cervio M, Faniglione M, de Angelis S, Pajoro M, Levandis G, *et al*. Intestinal dysmotility and enteric neurochemical changes in a Parkinson's disease rat model. Auton Neurosci 2012, 169: 77–86.
52. Zhang XL, Li Y, Liu CZ, Fan RF, Wang P, Zheng LF, *et al*. Alteration of enteric monoamines with monoamine receptors and colonic dysmotility in 6-hydroxydopamine-induced Parkinson's disease rats. Transl Res 2015, 166: 152–162.
53. Clairembault T, Leclair-Visonneau L, Coron E, Bourreille A, Le Dily S, Vavasseur F, *et al*. Structural alterations of the intestinal epithelial barrier in Parkinson's disease. Acta Neuropathol Commun 2015, 3: 12.
54. Sampson TR, Debelius JW, Thron T, Janssen S, Shastri GG, Ilhan ZE, *et al*. Gut microbiota regulate motor deficits and neuroinflammation in a model of Parkinson's disease. Cell 2016, 167: 1469-1480.e12.
55. D'Alessandro A, Moore HB, Moore EE, Reisz JA, Wither MJ, Ghasasbyan A, *et al*. Plasma succinate is a predictor of mortality in critically injured patients. J Trauma Acute Care Surg 2017, 83: 491–495.
56. Kumari S, Kumaran SS, Goyal V, Sharma RK, Sinha N, Dwivedi SN, *et al*. Identification of potential urine biomarkers in idiopathic Parkinson's disease using NMR. Clin Chim Acta 2020, 510: 442–449.
57. Tzimou A, Benaki D, Nikolaidis S, Mikros E, Taitzoglou I, Mougios V. Effects of lifelong exercise and aging on the blood metabolic fingerprint of rats. Biogerontology 2020, 21: 577–591.
58. Schapira AH, Cooper JM, Dexter D, Clark JB, Jenner P, Marsden CD. Mitochondrial complex I deficiency in Parkinson's disease. J Neurochem 1990, 54: 823–827.